SIAM J. IMAGING SCIENCES
Vol. 17, No. 1, pp. 389–414

The Cortical V1 Transform as a Heterogeneous Poisson Problem*

Alessandro Sarti†, Mattia Galeotti‡, and Giovanna Citti‡

Abstract. Receptive profiles of the primary visual cortex (V1) cortical cells are very heterogeneous and act by differentiating the stimulus image as operators changing from point to point. In this paper we aim to show that the distribution of cells in V1, although not complete to reconstruct the original image, is sufficient to reconstruct the perceived image with subjective constancy. We show that a color constancy image can be reconstructed as the solution of the associated inverse problem, which is a Poisson equation with heterogeneous differential operators. At the neural level the weights of short-range connectivity constitute the fundamental solution of the Poisson problem adapted point by point. A first demonstration of convergence of the result towards homogeneous reconstructions is proposed by means of homogenization techniques.

Key words. visual cortex, color constancy, Retinex, heterogeneous, Poisson equation, homogenization

MSC codes. 35H, 92B, 49K45, 49J55

DOI. 10.1137/23M1555958

1. Introduction.

The visual brain extracts more and more complex features starting from the visual stimulus. The cells of the retina and the lateral geniculate nucleus (LGN) extract the position of the contours, then the cells of the primary visual cortex (V1) extract the position and orientation of the image contours, up to the upper cortices where more complex features are extracted. The action of cells is characterized to a first approximation by linear receptive profiles (Ps) [25], called also "classical receptive profiles," which behave like filters representing the impulse response of the cells. Predictions of receptive profiles in V1 are in good agreement with receptive measurements reported in the literature (Hubel and Wiesel [25, 26, 27]; DeAngelis et al. [22, 23]). Specifically, explicit neurophysiological characterizations have been given of LGN neurons in terms of Laplacian of Gaussian, and simple cells in V1 have been compared to related models in terms of Gabor functions (Marcelja [37]; Jones and Palmer [28, 29]), differences of Gaussians (Rodieck [45]) or Gaussian derivatives (Koenderink and van Doorn [33]; Young [53]; Young et al. [54, 55]; Lindeberg [35]).

*Received by the editors February 27, 2023; accepted for publication (in revised form) July 19, 2023; published electronically February 21, 2024.
https://doi.org/10.1137/23M1555958
Funding: This work was funded under the National Recovery and Resilience Plan (NRRP), Mission 4 Component 2 Investment 1.3 - Call for Tender No. 341 of 15/03/2022 of Italian Ministry of University and Research funded by the European Union – Next GenerationEU Project code PE0000006, Concession Decree No. 1553 of 11/10/2022 adopted by the Italian Ministry of University and Research, CUP D93C22000930002, "A Multiscale Integrated Approach to the Study of the Nervous System in Health and Disease" (MNESYS). Also funded by GHAIA project, EUHorizon 2020 MSCA grant agreement 777822.
†CAMS, EHESS, Paris, France (alessandro.sarti@ehess.fr, http://cams.ehess.fr/alessandro-sarti/).
‡Dipartimento di Matematica, Università di Bologna, Bologna 40126, Italy (galeotti.mattia.work@gmail.com, giovanna.citti@unibo.it, https://www.dm.unibo.it/∼mattia.galeotti4/).

In several papers it has been shown that the set of profiles can be obtained through group transformations starting from a mother profile. For example, in [15] simple cell profiles of V1 were studied in the rotation and translation group, and it was shown that all the functional architecture related to these cells (horizontal connectivity and association fields) is to be considered as a direct consequence of the Lie group symmetries involved. This finding was extended to cells sensitive to scale in the symplectic group [48], to movement in the Galilean group [3], to curvature in the Engel group [1] and to rotation, scale, and frequency in the Heisenberg group [8]. The interested reader could refer to [17] for a complete review.

Simple cells sensitive to position and orientation are topographically organized in V1. The process of visual mapping from the retina to cortical neurons is known as retinotopy. Moreover in primates and cats, neurons with similar orientation selectivity are clustered together to constitute the so-called hypercolumnar [25] or pinwheel [11] organization. In the opposite, rodents do not have such specific feature organization as primates and cats. This means that the information encoded in V1 in rodents is distributed in a less organized fashion, known as "salt-and-pepper maps" [30]. Anyway, whatever the feature organization is, the three-dimensional group of rotations and translations of the plane is not completely represented since it is projected in the two-dimensional cortical surface of V1.

An important problem of contemporary neuroscience consists in understanding whether the perceived image can be reconstructed starting from the partial information carried by cells in V1. In other words, it is a question of understanding whether V1 is a high-resolution image buffer that contains the representation of the perceived image. In this sense V1 would make a cortical transform of the stimulus to obtain the perceived image.

In this regard, Barbieri in [4] shows that the distribution of receptive profiles in V1 is not complete, and therefore it is not sufficient to reconstruct the visual stimulus. Subsequently, he shows which additional constraints would be required to achieve the reconstruction.

In this paper we aim to show that the distribution of cells in V1, although not complete to reconstruct the original image, is sufficient to reconstruct the perceived image without additional constraints. In particular we focus on the perceptual phenomena of lightness constancy and color constancy, which are fundamental characteristics of the perceived image. Lightness constancy refers to the perception of an object's lightness as invariant with respect to the illumination conditions. Analogously, color constancy is a similar phenomenon, but this time is the perception of color resulting invariant with respect to illumination. We therefore aim to show that the distribution of cells in V1 is sufficient to perform a transform of the visual stimulus in the lightness and color constancy image perceived by the subject.

To do this we will consider the Ps as Gaussian derivatives [33, 53, 54, 55] with heterogeneous metrics and order of derivation. They act by differentiating the image as heterogeneous operators changing from point to point. Then we show that an image can be reconstructed as the solution of the associated inverse problem, which is a Poisson equation with heterogeneous operators. The homogeneous equivalent of this reconstruction is the Retinex differential model presented in [31, 39] in which the perceived image was obtained by first differentiating the stimulus with homogeneous Laplacian operators and then solving the associated inverse problem (Poisson equation). In our case we will generalize the Poisson equation to equations changing from point to point in order to reconstruct the perceived image. This kind of differential problem with heterogeneous operators was introduced, among others, in [49, 50] to

define the possibility of performing a differential calculus with operators that change from point to point in space and time.

Observe that the heterogeneous differential structure of images has been largely studied in the past, starting from the pioneering work of Koenderink [32]. A wide amount of studies about locally adaptive frames (or Gauge frames) has been developed and an exhaustive list of references has been collected in [6]. In this setting, detectors of features like edges, corners, t-junctions, ridges, monkey-saddles, and many more have been modeled by heterogeneous differential operators. A further expansion of heterogeneity has been provided by data-driven left-invariant metrics [5]. These works, although they underline the heterogeneity of the differential structure of images, concern the direct problem of differentiation and feature extraction rather than the inverse problem of stimulus reconstruction. On the other hand, research about stimulus reconstruction by inversion of differential operators are very few, and up to now they have dealt with homogeneous operators [38, 9, 10].

The originality of the present research is in performing operator inversion in a differential heterogeneous setting. We provide an existence result for weak solutions of the operator. A first proof of convergence of the result towards a homogeneous reconstruction as in [31, 39] will be proposed by means of homogenization techniques. The proof is constructed with operators discretized on regular grids (difference operators). We refer the reader in particular to [40, 34, 43] and develop the notion of H-convergence (see Definition 5.7) that was initially introduced by Spagnolo [51] and De Giorgi [20, 21]. Results of this kind for mathematical models of the cortex are, for example, [47, 14]. We consider a family of difference operators with random coefficients on an ε-spaced reticulum, and we prove that it can converge as $\varepsilon \to 0$ to a deterministic differential operator defined on a continuous domain and isotropic under a suitable hypothesis.

The paper is organized as follows. In section 2 some classical concepts of functional architecture of V1 are recalled. Classical models of receptive profiles are presented in terms of Gaussian derivatives and orientation maps of such profiles are shown both for hypercolumnar organization and salt-and-pepper maps. In section 3 the main model of cortical transform as a heterogeneous Poisson problem is presented. In section 4 we prove the existence of a weak solution of the problem using a steepest descent method. In the subsequent section 5 the notion of H-convergence is introduced and a sketch of the proof of convergence of the heterogeneous problem towards the homogeneous one is proposed. The main numerical results are shown and discussed in section 6.

2. Functional architecture of V1.

2.1. Receptives profiles. A receptive profile is the impulse response of a cell, which is the response of the cell to a delta of Dirac of a retinal stimulus. Statistical studies on the Ps of V1 cells in macaques show a great heterogeneity of behaviors [44]. Copies of center-surround Ps (Mexican hats) are present, as well as a great variety of simple cells with anisotropic Ps that detect orientation of boundaries, all with different orientation and frequency and many other complex cells.

In the simple case of Mexican hats the receptive profile will be denoted P_h (the index h denotes the fact that P is the profile of a Mexican hat); it is axial symmetric and in terms of Gaussian derivatives writes as

$$P_h(x_1, x_2) = \Delta G_\sigma(x_1, x_2), \tag{2.1}$$

where $x = (x_1, x_2)$ is the general point of the plane where G_σ is a two-dimensional Gauss function with variance σ and Δ is the Euclidean Laplacian.

In the case of receptive profiles of simple cells let's consider the directional derivative

$$X_{\theta,1} = \cos\theta \partial_{x_1} + \sin\theta \partial_{x_2}. \tag{2.2}$$

The receptive profile of a simple cell with preferred orientation $\theta + \pi/2$ writes as

$$P_s(x_1, x_2) = X_{\theta,1}^{2\beta} G_\sigma(x_1, x_2). \tag{2.3}$$

The coefficient β is always an integer, so that $X_{\theta,1}^{2\beta}$ denotes the directional derivative of order 2β in the direction θ. In particular this is a derivative of even order. Typically we will be interested in $\beta = 1$ or $\beta = 2$, giving rise to derivatives of order 2 or 4. The higher order derivative denotes the presence of a higher number of sinusoidal cycles under the Gauss bell [33] (see Figure 1).

2.2. Orientation maps. The preferred orientation of simple cells changes in the cortex point to point [25], giving rise to the so-called orientation map. The orientation map is a map $\theta : \mathbb{R}^2 \to [0, \pi]$, where $x = (x_1, x_2)$ are cortical coordinates and $\theta = \theta(x_1, x_2)$ is the preferred direction of columns of simple cells. In primates and cats, neurons with similar orientation selectivity are clustered together to constitute the so-called pinwheel organization [11]. A simple model of pinwheel-shaped orientation map is proposed in [42], where the map is obtained through the superposition of randomly weighted complex sinusoids:

$$\theta_1(x_1, x_2) = \arg \sum_{k=1}^{N} c_k e^{i2\pi(x_1 \cos(2\pi k/N) + x_2 \sin(2\pi k/N))}, \tag{2.4}$$

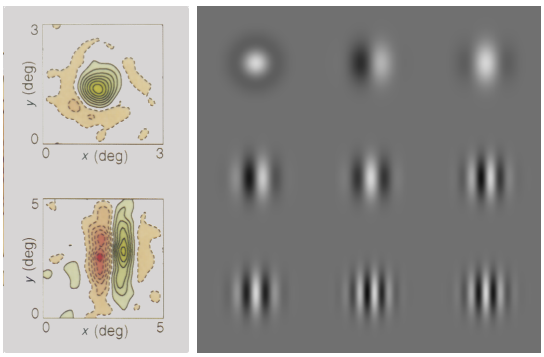

Figure 1. *Left: Receptive profiles of different kind of cells after neurophysiological measurement (inhibitory response in red, excitatory in yellow) as reported in [22] and [23]. Upper left: LGN receptive profiles show a characteristic center-surround response that can be modeled as a Laplacian of Gaussian. Bottom left: Simple cells of V1 show strong orientation preference and are modeled by directional derivatives of Gaussian. Right: Representation of Ps as derivatives of Gaussian of different degrees. (Left images ©1995 Elsevier. Reprinted, with permission, from [22].)*

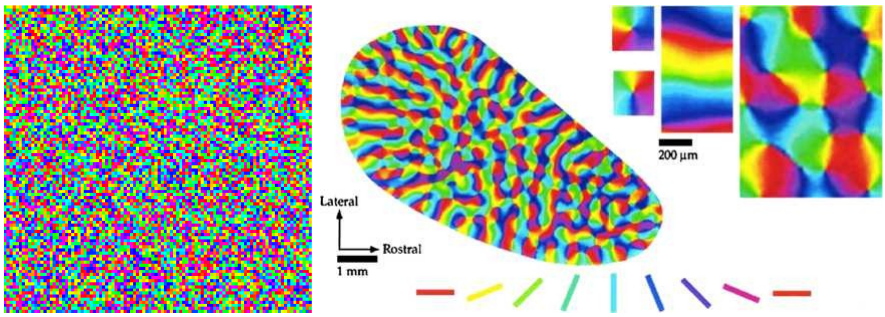

Figure 2. *Orientation maps in rodents are salt-and-pepper noise (left, our reconstruction), while in primates they present the so-called pinwheel structure (right, reproduced from* [12]*). A mathematical model of the two distributions is given, respectively, by* (2.5) *and* (2.4).

with N denoting the number of orientation samples and where the coefficients $c_k \in [0,1]$ are white noise. From (2.4) we obtain the so-called pinwheel structure, which is an orientation map with the presence of singularities around which all the orientations are present. The function is complex-valued and the color maps the argument of complex variables. The distance between singularities is almost constant. Pinwheel points are the two-dimensional implementation of a hypercolumn of orientations that is the set of orientations corresponding to a retinal point in the original model of Hubel and Wiesel [25] (see Figure 2).

In the opposite, in rodents the orientation information encoded in V1 is distributed in a less organized fashion, known as "salt-and-pepper maps" [30], and can be modeled by

$$\theta_2(x_1, x_2) = d(x_1, x_2), \tag{2.5}$$

where the coefficients $d \in [0, \pi]$ are white noise.

2.3. Short- and long-range connectivity. Cortical cells are reciprocally connected by short- and long-range connectivity. Short-range connectivity corresponds to the distribution of interaction between cells within a hypercolumn. On the other hand long-range connectivity induces interactions between hypercolumns. Long-range connectivity is very anisotropic and connects mainly cells with a similar orientation preference, while short-range connections are isotropic. Particularly, from neurophysiological measurements of the activity of pairs of V1 neurons, a correlation function is computed that is proportional to the functional connectivity between the pairs of units. This short-range connectivity show radial symmetry and a decrease in intensity proportional to $\log(r)$ or $1/r$ [19] (see Figure 3).

These connections are modulatory, meaning that they act on the output of Ps of cortical cells and not directly on the thalamic stimulus.

3. The cortical transform. We describe in the following the model for the coupled activity of classical receptive profiles and the short-range connectivity that modulates the feed-forward input giving rise to contextual modulation effects. Particularly the weights of local connectivity constitute the fundamental solution of a Poisson problem where the forcing term is given by the output of classical receptive profiles. This coupling can account for the lightness constancy of the perceived image (Retinex effect). Given the heterogeneity of cells linked by

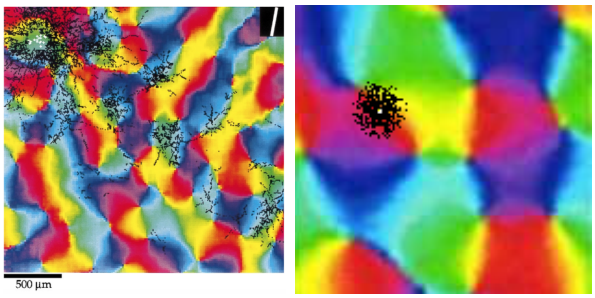

Figure 3. *Left: Long-range connectivity between hypercolumns from* [12]. *Right: Short-range connectivity within a hypercolumn (our representation from* [19]*).*

local connectivity, the model will end up in a Poisson equation with heterogeneous operators. Homogeneous version of the model can be found, for example, in [31] and [39], while a more complex model but without any image reconstruction is proposed by Cowan and Bressloff [13].

3.1. Feed-forward action on the input stimulus. The action of a classical receptive profile P on an input stimulus I writes as

$$O = P \star I,$$

where $\star$ is the convolution product and I is the image stimulus, on which the P acts as a linear filter. Particularly the action of Mexican reads

$$O_h = P_h \star I = \Delta G_\sigma \star I = \Delta I_\sigma, \tag{3.1}$$

where $I_\sigma = G_\sigma \star I$ is smooth approximation of I. The action of the simple cells P_s is written as

$$O_s = -(-1)^\beta X_{\theta,1}^{2\beta} G_\sigma \star I = -(-1)^\beta X_{\theta,1}^{2\beta} I_\sigma, \tag{3.2}$$

where β is a integer positive and even. For $\beta = 1$ the operator $X_{\theta,1}^{2\beta}$ is a second order directional derivative in the direction θ, which can be identified with a degenerate Laplacian. Let us recall that $-\Delta$ and $-X_{\theta,1}^2$ are elliptic.

Hence we postulate that the operator which acts on the image is different from one point to another and can be a random combination of the previous operators. In what follows we will always denote by L_Λ the considered linear operator, which can be $L_\Lambda = \Delta$ or $L_\Lambda = X_{\theta,1}^{2\beta}$, or a linear combination of them. We will be mostly interested in the values $\beta = 1$ and $\beta = 2$, which denote derivatives of order 2 or 4, respectively. The general operator will read

$$L_\Lambda = a_1 \Delta + a_2 X_{\theta,1}^2 - a_3 (-1)^\beta X_{\theta,1}^{2\beta} \tag{3.3}$$

for a partition of the unity a_i: at every point x one of these coefficients will take the value 1, and the others will vanish.

3.2. Reconstruction of the perceived image. The output of a distribution of V1 cells in response to the visual input I is the differentiation of the visual input itself. We will propose here a procedure to construct the perceived image by considering the integration of the operator. In previous papers, we conjectured that this step is accomplished by the action of the connectivity between V1 and LGN in a homogeneous setting [9, 10]. Here we clarify that it can be accomplished by short-range connectivity of V1 and by considering heterogeneous operators of V1.

Let's consider the inverse problem with respect to the differentiation $L_\Lambda I(x_1, x_2)$, which is the heterogeneous Poisson problem, with Neumann or Dirichlet conditions,

$$L_\Lambda u(x_1, x_2) = L_\Lambda I(x_1, x_2), \tag{3.4}$$

where the right-hand-side term is known and represents the action of receptive profiles on the visual input, while the solution u represents the reconstructed-perceived image. Equation (3.4) can be considered as an extension of a Poisson equation to heterogeneous operators. This process constructs the perceived image, which is the original input $I(x_1, x_2)$ up to a harmonic function. Clearly, harmonic no longer means the annulation of the Laplacian but rather the annulation of the heterogeneous operator L_Λ.

Having formalized the expression of the operator L_Λ we study the associated equation (3.4). Calling $f = L_\Lambda I$ the equation reduces to

$$L_\Lambda u = f \tag{3.5}$$

with Dirichlet or Neumann boundary conditions. We will prove the existence of solutions via parabolic approximation. Indeed we consider the evolution equation

$$\partial_t \tilde{u} = L_\Lambda \tilde{u} - f \tag{3.6}$$

with an arbitrary initial condition, and the same boundary condition as in (3.5) at any instant of time. Formally, for any open bounded domain Q we will introduce suitable Sobolev spaces $W^{1,2}_\Lambda(Q)$, we will consider L_Λ as an operator acting on the space and we will look at the Cauchy problem

$$\begin{aligned} &\tilde{u}' = L_\Lambda \tilde{u} - f, \\ &u(0) \in W^{1,2}_\Lambda(Q) \end{aligned} \tag{3.7}$$

(the initial condition vanishes at the boundary if we consider a Dirichlet problem). We will see under which condition the Cauchy problem is defined for every instant of time, there exists $\lim_{t\to\infty} \tilde{u}$ and the limit coincides with the solution u of (3.5).

4. Existence of weak solutions. The operator defined in (3.3) is degenerate when $a_1 = a_3 = 0$, even if θ is constant. Indeed, if $\theta = 0$, the equation reduces to

$$\partial^2_{x_1 x_1} u = f$$

in an open set $Q \subset \mathbb{R}^2$, so that it is not uniformly elliptic. In addition it is of order 2 at some points, and of order 4 at other points. We will formalize the definition of solutions in suitable Sobolev spaces associated to the considered directional derivatives. In addition, we will prove the convergence of the solution of the parabolic equation (3.6) to the solution to problem (3.5).

4.1. Definition of weak solution. We would like to introduce a definition of a differential operator sufficiently flexible to cover the Euclidean Laplacian and the degenerate Laplacian defined in (3.3). To this end we will consider a smooth manifold Q locally diffeomorphic to $\mathbb{R}^2$, and we will define a subbundle H of the tangent bundle TM of Q. Then we define a metric g on H. The triple (Q, H, g) is called sub-Riemannian manifold. By definition of metric, for every x the metric g defines a scalar product on the horizontal tangent plane H_x.

4.2. Second order operators. At every point x the horizontal tangent space H_x will be defined by the choice of generators Λ_x. The expression of Λ_x will reflect the choice of receptive profiles at that point. As a consequence we will choose as set of generators

$$\Lambda_x = \{z_1, z_2\}, \text{ where } z_1 = a_1(\cos(\theta(x)), \sin(\theta(x))),\ z_2 = a_2(-\sin(\theta(x)), \cos(\theta(x))). \tag{4.1}$$

The dimension of the generated horizontal tangent space will depend on the zeros of the functions a_i and can be 1 or 2. Correspondingly, in addition to the vector field $X_{\theta(x),1}$ introduced in (2.2) we define a second vector field to complete the basis of the space,

$$X_{\theta(x),1} = \cos(\theta(x))\partial_{x_1} + \sin(\theta(x))\partial_{x_2},\ X_{\theta(x),2} = -\sin(\theta(x))\partial_{x_1} + \cos(\theta(x))\partial_{x_2}, \tag{4.2}$$

and we will work with the vector fields $a_i X_{\theta(x),i}$.

For any bounded set $Q \subset \mathbb{R}^d$ and every $h \in C_0^\infty$, we define the horizontal gradient

$$\nabla_\Lambda h := \sum_{i=1}^{2} X_{\theta(x),i} h X_{\theta(x),i}.$$

This allows us to define the integral norm

$$\|h\|_{W^{1,2}_\Lambda(Q)} = \sqrt{\sum_{i,j=1}^{2} \int_Q a_i^2 (X_{\theta(x),i} h)^2(x) dx}.$$

The Sobolev space $W^{1,2}_{0,\Lambda}(Q)$ will be the closure of $C_0^\infty(Q)$ with respect to this norm. If Q is smooth, $W^{1,2}_\Lambda(Q)$ is the set of functions h whose norm $\|h\|_{W^{1,2}_\Lambda(Q)}$ is bounded. Recall that the coefficients a_i can vanish, making the space degenerate. By definition the following Dirichlet functional is well defined in the space $W^{1,2}_\Lambda(Q)$:

$$F(u) = \sum_{i=1}^{2} \int_Q a_i^2 (X_{\theta(x),i} u)^2(x) dx. \tag{4.3}$$

If X is an arbitrary operator of second order with differentiable coefficients, we call the *formal adjoint of* X the operator X^* defined by the relation

$$\int_Q Xuh = \int_Q uX^* h \quad \forall u \in W^{1,2}_\Lambda(Q), h \in C_0^\infty(Q).$$

The associated Laplacian is formally defined as

$$L_\Lambda u = \sum_{i=1}^{2} X^*_{\theta(x),i} (a_i^2 X_{\theta(x),i} u). \tag{4.4}$$

By definition of formal adjoint, the weak solution is defined as follows.

Definition 4.1. *Let Q be a bounded open set. A function $u \in W^{1,2}_{\Lambda}(Q)$ is a weak solution of the equation $L_\Lambda u = f \in L^2(Q)$ if for every smooth function h compactly supported in Q*

$$\int_Q \sum_{i=1}^{2} a_i^2 X_{\theta(x),i} u X_{\theta(x),i} h dx = -\int_Q f h dx,$$

where a_i are bounded and measurable. The function u attains the value 0 at the boundary in a weak sense if $u \in W^{1,2}_{0,\Lambda}(Q)$. It attains the Neumann boundary datum if it is the minimum of the associated functional

$$J(u) = F(u) - \int_Q f u. \tag{4.5}$$

4.3. Higher order operators. We already noted that the operator defined in (3.3) can have order greater than 2 or can be a linear combination of operator of different order. In the simplest case the operator reduces to

$$L_\Lambda u(x) = X^*_{\theta(x),1}(a_1^2 X_{\theta(x),1})u(x) - (X^2_{\theta(x),1})^*(a_3^2 X^2_{\theta(x),1})u(x). \tag{4.6}$$

In order to simplify the proof, we will consider the operator

$$L_\Lambda u(x) = X^*_{\theta(x),1}(a_1^2 X_{\theta(x),1} u)(x) - \Delta(a_3^2 \Delta)u(x), \tag{4.7}$$

which can have different order at different points. Observe that $L_\Lambda = -dF$, where F is the operator

$$F(u) = \sum_{i=1}^{2} \int_Q a_i^2 (X_{\theta(x),i} u)^2(x) dx + \int_Q a_3^2 (\Delta^2 u)^2(x) dx. \tag{4.8}$$

As before, this functional, well defined on functions $u \in C_0^\infty$, defines the square of a norm. The closure of C_0^∞ with respect to this norm defines a Sobolev space where the associated equation is well defined. If $a_3 = 0$, the operator reduces to a second order operator, which can be degenerate or not. If $a_i = a_2 = 0$, $a_3 = 1$, the operator reduces to the bi-Laplacian, denoted by Δ_E^2. We have defined an operator L_Λ heterogeneous both in its differential order and in the type of metric.

4.4. Existence of a solution. In all the considered problems, the operator L_Λ is the differential of a functional J defined on a suitable Hilbert space S of Sobolev type. We will show that in this case the solution of the stationary problem can be obtained via the steepest descent method.

Precisely assume that Q is a bounded domain subset of $\mathbb{R}^2$. Also assume that J is of class $C^{1,1}(S)$. By the Riesz representation theorem there exists a function $\nabla J(u) \in S$ such that $dJ(u)(h)$ admits the following representation with respect to the scalar product of the space S $dJ(u)(h) = \langle \nabla J(u), h \rangle$. Assume that $Lu - f = -\nabla J(u)$, so that problem (3.7) reduces to

$$\begin{aligned} &\tilde{u}' = -\nabla J(\tilde{u}), \\ &\tilde{u}(0) \in S. \end{aligned} \tag{4.9}$$

Remark 4.2. If $J \in C^{1,1}$ and it is bounded below, then $-\nabla J(u)$ is Lipschitz continuous and the Cauchy problem (4.9) is well defined. Due to the boundedness from below of J, its solution is defined on $[0, \infty[$.

We will need the following compactness assumption of Palais–Smale (PS) type.

Definition 4.3. *A functional J satisfies the PS condition at the level m if for every sequence u_n such that*

$$J(u_n) \to m, \quad dJ(u_n) \to 0$$

the sequence u_n has a converging subsequence.

Theorem 4.4 (see [2]). *If J is convex, is of class $C^{1,1}$, satisfies the PS condition, and is bounded below, there exists $\lim_{t\to\infty} \tilde{u} = u$ and u is a minimum of the functional J. In particular it satisfies $dJ(u) = 0$.*

These results can be directly applied to the functionals we have introduced and will be intensively used in the next sections.

Example 4.5. We consider the functional J defined as in (4.5) on the Sobolev space $W^{1,2}_{0,\Lambda}$. Here we assume that θ is measurable, and a_i are measurable and bounded. Then the functional is of class $C^{1,1}$ and its differential is

$$dJ(u)(h) = dF(u)(h) - \int_Q fh = \int_Q \sum_{i=1}^{2} a_i^2 X_{\theta(x),i} u X_{\theta(x),i} h - \int fh. \tag{4.10}$$

If both a_i are different from 0, the convergence of the steepest descent method is known.

If $a_1 = 1$, $a_2 = 0$, and $\theta(x, y)$ is a C^1 approximation of one of the functions defined in (2.4) or (2.5), the operator is totally degenerate. In this case we recover the operator (3.2) associated to V1 receptive profiles. Also, in this case it is possible to prove the PS condition. Indeed, if we consider a sequence such that $dJ(u_n)(h) \to 0$ and $J(u_n) \to \inf_{W^{1,2}_{0,\Lambda}} J$, then $\|u_n\|^2_{W^{1,2}_{0,\Lambda}}$ is bounded, so that there is a function $u \in W^{1,2}_{0,\Lambda}$ such that u_n weakly converges to u in $W^{1,2}_{0,\Lambda}$ and u_n weakly converges to u in L^2. From $dJ(u_n) \to 0$ we also deduce that $dJ(u_n)(u_n) \to 0$, so that

$$\lim_n \|u_n\|^2_{W^{1,2}_{0,\Lambda}} = \lim_n \int f u_n = \int fu$$

for the weak convergence. From the assumption of the differential we also know that $dJ(u_n)(u) \to 0$, so that

$$\|u\|^2_{W^{1,2}_{0,\Lambda}} = \lim_n \int_Q X_{\theta(x),1} u_n X_{\theta(x),1} u = \int fu.$$

It follows that $u_n \to u$ weakly in $W^{1,2}_{0,\Lambda}$ and $\|u_n\|^2_{W^{1,2}_{0,\Lambda}} \to \|u\|^2_{W^{1,2}_{0,\Lambda}}$, which implies the convergence of u_n to u in $W^{1,2}_{0,\Lambda}$.

As a consequence, by Theorem 4.4 the solutions of the stationary problems are the limit of the solution of the parabolic one.

Example 4.6. The operator in (4.7) is the differential of the functional

$$J(u) = \sum_{i=1}^{2} \int_Q a_i^2 (X_{\theta(x),i} h)^2(x) dx + \int_Q (\Delta u)^2(x) dx - \int_Q f(x) u(x).$$

As before, this operator satisfies the PS condition. Indeed, a sequence such that $dJ(u_n) \to 0$ and $J(u_n) \to \inf J$ has the Laplacian bounded in L^2, so that, arguing as before, we obtain the convergence of u_n. The assumptions of Theorem 4.4 are satisfied, which ensures that the solution obtained through the parabolic approximation tends to the solution of the fourth order operator.

We applied here the steepest descent method; the main limitation of the method is that it can be applied only to minima of functionals. However, it has the big advantage that it can be applied to degenerate operators such as the one in Example 4.5, since the functional, while approximating a minimum, bounds the norm of the minimizing sequence. Other powerful methods, such as, for example, the semigroup technique, allow one to handle the case where the equation does not come from a minimum of a functional. However, the convergence result requires that the biggest eigenvalue of the operator be negative, which is not the case of the degenerate operators in Example 4.5.

4.4.1. The Green function. The previous method allows us to find the Green function of the operator L_Λ in open, smooth sets $Q \subset \mathbb{R}^d$. The Green function is a smooth kernel $\Gamma : Q \times Q \backslash \{(x,x) : x \in Q\} \to \mathbb{R}$ such that any solution of the problem

$$L_\Lambda u = f \text{ in } Q, \quad \partial_\nu u = 0 \text{ on } \partial Q$$

can be represented in the form

$$u(x) = -\int_Q \Gamma(x,y) f(y) dy.$$

For a large class of operators with measurable coefficients analogous to L_Λ, the existence of a Green function, or fundamental solution (which is the analogous kernel on the whole space), is known. In [24] this is proved for second order uniformly elliptic operators, while the existence of a fundamental solution for uniformly subelliptic operators is due to [46].

If we fix the first entry $x \in Q$, the Green function as a function of its second entry is a smooth function $\Gamma(x,-) : Q \backslash \{x\} \to R$ solution of the problem

$$L_\Lambda^* \Gamma(x,-) = \delta_x \text{ in } Q, \quad \partial_\nu \Gamma = 0 \text{ on } \partial Q,$$

where L_Λ^* is the formal adjoint of L_Λ.

In order to solve this last problem and find the Green function, we can apply the steepest descent method we have introduced (see also results in section 6).

5. Discretization and homogenization results. The aim of this section is to provide homogenization results for operators of the same type as those defined in (3.3) and (4.4). We can express the theory in an open set $Q \subset \mathbb{R}^d$. To this end we will consider a finite set $\Lambda \subset \mathbb{Z}^d$ symmetric with respect to 0, and we will call m the number of its elements. Any element z_i with $i = 1, \dots, m$ is a vector, and the associated directional derivative will be denoted by $X^\varepsilon_{z_i}$. We intend to study the discretization of the following Dirichlet problem, which generalizes the operator (4.4) defined above:

$$-\sum_{i=1}^{m} (X^\varepsilon_{z_i})^* \left(a_{ij}(x) X^\varepsilon_{z_j} u(x) \right) = f(x). \tag{5.1}$$

We will consider both deterministic and stochastic coefficients a_{ij}. For deterministic coefficients we study the convergence of the discretized problem to the continuous one. In the stochastic case, we show that, even if we start with a random orientation θ in the discrete problem, a homogenization procedure will ensure the convergence to a continuous problem with constant coefficients.

5.1. Difference operators. We recall here how to discretize this second order differential operator, referring the reader to [40] and [43] for a wider introduction.

We start with discretizing a smooth bounded domain $Q \subset \mathbb{R}^d$. Let us call $Q_\varepsilon = Q \cap \varepsilon \mathbb{Z}^d$, where $\varepsilon > 0$. The boundary $\partial Q^\Lambda_\varepsilon$ of Q_ε is defined by

$$\partial Q^\Lambda_\varepsilon := \{x + \varepsilon z_i |\ x \in Q_\varepsilon,\ i = 1, \dots, m\} \backslash Q_\varepsilon.$$

We also introduce $\overline{Q}_\varepsilon := Q_\varepsilon \cup \partial Q^\Lambda_\varepsilon$.

Consider a function $u^\varepsilon \colon Q_\varepsilon \to \mathbb{R}$; then the standard difference operator associated by $X^\varepsilon_{z_i}$ is defined by

$$X^\varepsilon_{z_i} u^\varepsilon(x) := \frac{u^\varepsilon(x + \varepsilon z_i) - u^\varepsilon(x)}{\varepsilon} \quad \forall i = 1, \dots, m.$$

We explicitly note that z_i is a vector, not necessarily an element of the canonical basis, of the space, so that in general $X^\varepsilon_{z_i}$ represents the discretization of the directional derivative X_i, not a partial derivative.

Here we can consider a matrix $A^\varepsilon(x) = (a^\varepsilon_{ij}(x))_{ij=1,\dots,m}$ when $x \in Q_\varepsilon$. With this notation, the discrete Laplace operator can be written as follows:

$$L^\varepsilon_\Lambda u^\varepsilon(x) := \sum_{i=1}^{m} X^\varepsilon_{-z_i} (a^\varepsilon_{ij}(x) X^\varepsilon_{z_i} u^\varepsilon(x)). \tag{5.2}$$

Consequently, the Dirichlet problem with second member $f^\varepsilon \colon Q_\varepsilon \to \mathbb{R}$ becomes

$$L^\varepsilon_\Lambda u^\varepsilon(x) = f^\varepsilon(x) \quad \forall x \in Q_\varepsilon, \tag{5.3}$$

with $u^\varepsilon(x) = 0$ if $x \in \partial Q^\Lambda_\varepsilon$.

Definition 5.1. *We say that problem (5.3) is uniformly elliptic if there exist constant* $c_1, c_2, \varepsilon_0 > 0$ *such that for any* $\eta \in \mathbb{R}^d$ *represented as* $\eta = \sum_{i=1}^m \eta_i z_i$ *one has*

$$|a_{ij}^\varepsilon(x)| \le c_1 \quad \forall x \in \overline{Q}_\varepsilon \ \forall i,j = 1,\dots,m, \tag{5.4}$$

$$c_2 \cdot \|\eta\|_E^2 \le \sum_{i,j=1}^m a_{i,j}^\varepsilon(x)\eta_i\eta_j \ \forall x \in \overline{Q}_\varepsilon, \tag{5.5}$$

where $\|\eta\|_E$ *is the Euclidean norm.*

Let us now define suitable functional spaces where we will look for the solution. We consider $v^\varepsilon : \varepsilon\mathbb{Z}^d \to \mathbb{R}$, and we define the analogue of the L^2-norm as

$$\|u^\varepsilon\|^2_{L^2(Q_\varepsilon)} := \varepsilon^d \sum_{x \in Q_\varepsilon} |v^\varepsilon(x)|^2.$$

If we consider $v^\varepsilon : \varepsilon\mathbb{Z}^d \to \mathbb{R}$, we say that v^ε is in $W_0^{1,2}(Q_\varepsilon)$ if $v^\varepsilon(x) = 0$ for any $x \notin Q_\varepsilon$; this is in fact a translation of the notion of Sobolev space to the discrete setting. The notion of discrete gradient descends from this setting straightforwardly.

Definition 5.2. *Consider* $v^\varepsilon \in W_0^{1,2}(Q_\varepsilon)$,

$$\nabla_\Lambda^\varepsilon v^\varepsilon(x) := \sum_{j=1}^m X_{z_j}^\varepsilon v^\varepsilon(x) X_{z_j}^\varepsilon \quad \forall x \in \overline{Q}_\varepsilon.$$

Due to the uniform ellipticity condition, we can choose the following norm on $W_0^{1,2}$:

$$\|v^\varepsilon\|^2_{W_0^{1,2}(Q_\varepsilon)} := \varepsilon^d \cdot \sum_{x \in \overline{Q}_\varepsilon} \sum_{i=1}^m, \left| X_{z_j}^\varepsilon v^\varepsilon(x) \right|^2.$$

We denote by $W^{-1,2}(Q_\varepsilon)$ the dual space to $W_0^{1,2}(Q_\varepsilon)$.

We will provide a definition of solutions of the equation of the operator L_Λ^ε generalizing to the discrete setting a mean value formula. Indeed it is well known that if Δ is the standard Laplacian, $B(x,\varepsilon)$ is the ball of radius ε, and $|B(x,\varepsilon)|$ is its Lebesgue measure, then

$$u(x) - \frac{1}{|B(x,\varepsilon)|} \int_{B(x,\varepsilon)} u(y)dy = \frac{\varepsilon^2}{4+2d}\Delta u + o(\varepsilon^2) \text{ as } \varepsilon \to 0.$$

The same formula still holds for large classes of linear operators.

In the discrete setting we will consider the following formula introduced in [43, Proposition 1.3].

Proposition 5.3. *Consider a function* $p_{z_i}^\varepsilon : Q_\varepsilon \to \mathbb{R}$ *defined for any* $z_i \in \Lambda$ *if it satisfies the following three properties:*

1. $p_{z_i}^\varepsilon(x) \ge 0$ *and* $\sum_{i=1}^m p_{z_i}^\varepsilon(x) = 1 \ \forall x \in Q_\varepsilon$*;*
2. $\exists \delta > 0$ *such that* $p_{\pm e_i}^\varepsilon \ge \delta$ *for* $i = 1,\dots,d$*;*
3. $p_{z_i}^\varepsilon(x) = p_{-z_i}^\varepsilon(x + \varepsilon z_i)$.

Then the following problem is uniformly elliptic:

$$u^\varepsilon(x) - \sum_{i=1}^{m} p^\varepsilon_{z_i}(x) u^\varepsilon(x + \varepsilon z_i) = \varepsilon^2 \cdot f^\varepsilon(x) \ \text{ in } Q_\varepsilon, \quad u^\varepsilon(x) = 0 \ \forall x \in \partial Q^H_\varepsilon, \tag{5.6}$$

for any $f^\varepsilon : Q_\varepsilon \to \mathbb{R}$.

Remark 5.4. The operator associated to the previous mean value formula can be rewritten in the form (5.3) with $a^\varepsilon_{ij}(x) = p^\varepsilon_{z_i}(x)$ if $z_i = z_j \neq 0$, and 0 otherwise.

In order to compare the functions defined over Q_ε with those having a continuous argument, we follow Kozlov [34] in defining a mesh completion. In particular if $f^\varepsilon : Q_\varepsilon \to \mathbb{R}$, then we denote by $\tilde{f}^\varepsilon : Q \to \mathbb{R}$ the function such that

$$\tilde{f}^\varepsilon(x) = f(y_x) \ \ \forall x \in Q,$$

where y_x is the point in Q_ε of components $y_x = (y_1, \dots, y_d)$ such that

$$y_i - \frac{\varepsilon}{2} \leq x_i < y_i + \frac{\varepsilon}{2} \ \ \forall i = 1, \dots, d.$$

In what follows, if it is clear from the context, we will allow some abuse of notation by denoting $\tilde{f}^\varepsilon \in W^{1,2}_0(Q)$ also by f^ε. Furthermore, we will say that f^ε converges (strongly or weakly) to f in $L^2(Q_\varepsilon)$, $W^{1,2}(Q_\varepsilon)$, or $W^{-1,2}(Q_\varepsilon)$ when the mesh completion $\tilde{f}^\varepsilon$ converges to f in $L^2(Q)$, $W^{-1,2}(Q)$. If needed, we will replace this mesh completion with a piecewise linear one $\tilde{f}^\varepsilon$ in $W^{1,2}(Q)$. In this case we will say that f^ε converges (strongly or weakly) to f in $W^{1,2}(Q_\varepsilon)$ if the piecewise linear mesh completion $\tilde{f}^\varepsilon$ converges to f in $W^{1,2}(Q)$.

5.2. Convergence results—deterministic model. We are interested in treating the convergence of difference operators to usual differential operators when imposing $\varepsilon \to 0$. We start by considering an existence result and its uniform estimates.

Proposition 5.5. *If problem (5.3) is uniformly elliptic and* $f^\varepsilon \in L^2(Q_\varepsilon)$*, then there exists a unique solution of the problem* $u^\varepsilon \in W^{1,2}_0(Q_\varepsilon)$ *and there exists* $c > 0$ *such that*

$$\|u^\varepsilon\|_{W^{1,2}_0} \leq c \cdot \|f^\varepsilon\|_{L^2},$$

uniformly in ε.

In what follows we denote as usual by $\rightharpoonup$ the weak convergence. The weak convergence of difference operators preserves in fact the notion of partial derivative.

Proposition 5.6 ([34, p. 355]). *If* $u^0 \in W^{1,2}_0(Q)$ *(or* $L^2(Q)$*) and* $u^\varepsilon \rightharpoonup u^0$ *in* $W^{1,2}_0(Q_\varepsilon)$ *(or* $L^2(Q_\varepsilon)$*), then*

$$X^\varepsilon_{e_i} u^\varepsilon \rightharpoonup \frac{\partial u^0}{\partial e_i} \ \ \text{in } L^2(Q_\varepsilon) \text{ or } W^{-1,2}(Q_\varepsilon).$$

We will denote by A an uniformly elliptic matrix and by A^ε its discretization on the ε grid. Consider a family of uniformly elliptic discrete Dirichlet problems (5.3). As before we denote by $A^\varepsilon(x)$ the coefficient matrix. We will also denote by $A(x)$ an $m \times m$ real matrix defined for $x \in Q$, whose coefficients will be denoted by a_{ij}.

Denote by u^ε the solution of the Dirichlet problem associated to u^ε and by u^0 the solution of the continuous Dirichlet problem (5.1).

Definition 5.7. *We say that the matrix A^ε H-converges to A, $A^\varepsilon \xrightarrow[\varepsilon\to 0]{H} A$, if for any sequence $f^\varepsilon \in W^{-1,2}(Q_\varepsilon)$ such that $f^\varepsilon \to f \in W^{-1,2}(Q)$ we have*

$$u^\varepsilon \rightharpoonup u^0 \text{ in } W_0^{1,2}(Q_\varepsilon),$$
$$D_{a^\varepsilon} u^\varepsilon = \sum_{j=1,\dots,m} a_{ij}^\varepsilon X_j^\varepsilon u^\varepsilon \rightharpoonup D_a u^0 = \sum_{j=1}^m a_{ij} X_j u^0 \text{ in } L^2(Q_\varepsilon).$$

Definition 5.8. *Given a matrix-valued function $A^1(x) = (a_{ij}^1(x))$ with $i,j = 1,\dots,m$ and $x \in \mathbb{Z}^d$, and a sequence of induced matrices $A^\varepsilon(x) := A^1(x/\varepsilon)$ for any $x \in Q_\varepsilon$, if the associated problem (5.3) is uniformly elliptic and there is a constant matrix A^0 such that $A^\varepsilon \xrightarrow{H} A^0$, then we call the matrix A^0 the homogenized matrix for A^ε.*

5.3. Convergence results—stochastic model. We will now consider an operator with random coefficients, similar to the one introduced in (2.5) and in section 4.2 to describe the action of the receptive profiles.

In order to treat the case of random coefficients, consider a probability space $(\Omega, \mathcal{F}, \mu)$ and a group $\{T_x \colon \Omega \to \Omega |\ x \in \mathbb{Z}^d\}$ of $\mathcal{F}$-measurable transformations respecting the following properties:

1. $T_x \colon \Omega \to \Omega$ is $\mathcal{F}$-measurable $\forall x \in \mathbb{Z}^d$;
2. $\mu(T_x \mathcal{B}) = \mu(\mathcal{B})$ $\forall \mathcal{B} \in \mathcal{F}$ and $\forall x \in \mathbb{Z}^d$;
3. $T_0 = \mathrm{id}$ and $T_x \circ T_y = T_{x+y}$ $\forall x, y \in \mathbb{Z}^d$.

Definition 5.9. *The group T_x is ergodic if for any $f \in L^1(\Omega)$ such that $f(T_x\omega) = f(\omega)$ for μ-a.e. $\omega \in \Omega$ and for any $x \in \mathbb{Z}^d$, there exists a constant K such that μ-a.s. $f = K$.*

In what follows we suppose the group T_x to be ergodic and we build a family of random operators. Consider an $\mathcal{F}$-measurable function with matrix values $\mathcal{A}(\omega) = (a_{ij}(\omega))$ for $\omega \in \Omega$ such that $\mathcal{A}$ is an $m \times m$ symmetric matrix. We define the family of operators

$$A^\varepsilon(x)(\omega) := \mathcal{A}(T_{x/\varepsilon}\omega) \quad \forall \omega \in \Omega, x \in \varepsilon\mathbb{Z}^d.$$

Remark 5.10. We state a condition on $\mathcal{A}$ that implies the uniform ellipticity of the family A^ε. Consider $\eta \in \mathbb{R}^d$ represented as $\eta = \sum_{i=1}^m \eta_i z_i$. If there exist $c_1, c_2 > 0$ such that the inequalities

$$|a_{ij}(\omega)| \le c_1,$$
$$c_2 \cdot \|\eta\|_E \le \sum_{z_i, z_j \in \Lambda \setminus \{0\}} a_{ij}^\varepsilon(\omega)\eta_i\eta_j, \ \forall x \in Q_\varepsilon$$

for all $\eta \in \mathbb{R}^d$ represented as $\eta = \sum_{i=1}^m \eta_i z_i$ are true a.s., then the A^ε are uniformly elliptic in any regular domain Ω.

Theorem 5.11 ([43, Theorem 2.17]). *If the operators A^ε are built as above, with T_x ergodic group and the matrix $\mathcal{A}$ respecting the conditions of Remark 5.10, then a.s. the family A^ε admits a homogenization and the homogenized matrix A^0 does not depend on ω.*

Let us now apply our theoretical results to (2.5), and to the choice of orientation (2.4) under the simplified assumption that the only possible directions are vertical or horizontal.

We consider a particular family of operators A^ε and analyze its asymptotic behavior. In particular we work in dimension $d=2$ and use some results of percolation theory in order to show that for some well-defined families, the operator converge asymptotically to a Laplacian.

Randomly chosen horizontal or vertical orientation. We split $\mathbb{R}^2$ into squares $\{[-\frac{1}{2},\frac{1}{2}] + j |\ j \in \mathbb{Z}^2\}$ and consider a random variable κ_r defined over $\mathbb{R}^2$, such that if $\delta > 0$, then

$$\kappa_r = \begin{cases} \delta & \text{with probability } r, \\ 1 & \text{with probability } 1-r, \end{cases}$$

where $0 < r < 1$. Given a finite subset $\Lambda \subset \mathbb{Z}^2$ symmetric with respect to 0, we consider the transition functions $p_{z_i}(x)$ for any $x \in \mathbb{R}^2$ and $z_i \in \Lambda$, and suppose the $p_{z_i}(x)$ are functions defined on the set $\{\kappa_r(x+z_i) |\ z_i \in \Lambda\}$.

The independence of $\kappa_r(j)$ for different $j \in \mathbb{Z}^2$ implies that the transformation group allowing the construction of the families $\{p_{z_i}(x) |\ x \in \mathbb{R}^2\}$ is ergodic, or equivalently that if $\forall z_i \in \Lambda$ if $p_{z_i}(x) = p_{z_i}(0)$ a.s., then a.s. p_{z_i} equals a constant.

From the $p_{z_i}(x)$ we define the transition functions $p^\varepsilon_{z_i}(x)$ in order to describe a uniformly elliptic problem as in (5.6),

$$p^\varepsilon_{z_i}(x) := p_{z_i}(x/\varepsilon) \quad \forall x \in Q_\varepsilon \subset \varepsilon\mathbb{Z}^2.$$

The operators $A^\varepsilon = (a^\varepsilon_{ij})$ are defined by $a^\varepsilon_{ii}(x) = p^\varepsilon_{z_i}(x)$ if $z_i \neq 0$, and $a^\varepsilon_{ij}(x) = 0$ otherwise.

Proposition 5.12 ([34, sect. 2]). *If the functions $p^\varepsilon_{z_i}$ built as above satisfy a.s. the three hypotheses of Proposition 5.3, then the A^ε H-converge a.s. to an elliptic operator A^0 with constant coefficients, and moreover A^0 is isotropic,*

$$A^0 = (a^0_{ij}) = a^\delta(r) \cdot id,$$

where $a^\delta(r) \in \mathbb{R}$.

The work [43] focuses on the case where the functions p_{z_i} are defined by

$$p_{z_i}(x) := \begin{cases} \frac{2\kappa_r(x)\cdot\kappa_r(x+z_i)}{4(\kappa_r(x)+\kappa_r(x+z_i))} & \text{if } z_i \in \Lambda\backslash\{0\}, \\ 1 - \sum_{z_i \neq 0} p_{z_i}(x) & \text{if } z_i = 0. \end{cases}$$

Second and higher order operators. Let us explicitly state that the convergence theory developed up to this point can be applied only to second order operators. It is not clear if similar results could be obtained for operators of order different from one point to another.

6. Results. The reconstruction model of (3.4) is implemented by numerically solving the parabolic equation (3.6),

$$u_t = L_\Lambda u - L_\Lambda I, \tag{6.1}$$

with the heterogeneous operator L_Λ given by (3.3) and $\beta = 2$, so that to take into account three main kind of receptive profiles, we have the following:

$$L_\Lambda = a_1\Delta + a_2 X^2_{\theta,1} - a_3 X^4_{\theta,1}. \tag{6.2}$$

The spatial domain Q is discretized with uniform spacing ε to obtain the matrix Q_ε on which the solution u^ε is defined. Centered finite differences are used to approximate spatial derivatives of the Laplacian

$$\Delta = \partial^2_{x_1x_1} + \partial^2_{x_2x_2}$$

as well as the second ordered sub-Riemannian term

$$X^2_{\theta,1} = \cos^2(\theta)\partial^2_{x_1x_1} + 2\cos(\theta)\sin(\theta)\partial^2_{x_1x_2} + \sin^2(\theta)\partial^2_{x_2x_2},$$

where (x_1, x_2) denotes a point in Q_ε. The fourth order sub-Riemannian term is computed by applying twice the second order term,

$$X^4_{\theta,1} = X^2_{\theta,1}(X^2_{\theta,1}).$$

Time evolution is discretized with forward finite difference, and Neumann boundary conditions are applied. A typical time step of the evolution is $dt = 0.1$ if just second order operators are involved, while $dt = 0.001$ is adopted if fourth order operators are present, in order to guarantee the stability of a finite difference method [52, p. 26]. The stopping criterion is directly related to the error of convergence of the solution so that the evolution stops when $\sum_{x\in Q_\varepsilon} |u^\varepsilon_{k+1}(x) - u^\varepsilon_k(x)| < \varepsilon_c$, where u^ε_k and u^ε_{k+1} are solutions corresponding to two subsequent time steps and $\varepsilon_c = 10^{-4}$.

The three bands of the RGB image stimulus shown in Figure 4 (left) have been processed separately. Different mixtures of second and fourth order operators in Euclidean and sub-Riemannian metrics have been considered by changing the parameters a_1, a_2, a_3.

In our first numerical test, only isotropic Laplacians have been considered (Figure 5) setting $a_1 = 1, a_2 = 0, a_3 = 0$. The set of Ps are visualized in a subsampled set of points (upper left) and they are all equal. Equation (3.4) corresponds in this case to the classical Poisson problem introduced by Morel to solve the Retinex algorithm with differential instruments [39]. The solution is visualized (bottom right) and corresponds to the image stimulus up to a harmonic function. The Green function $\Gamma(x_1, x_2)$ (see section 4.4.1) is computed for some points γ. Its level lines are visualized (upper right) as well as its surface (bottom left). In

Figure 4. *Original painting of Piero della Francesca (left) and its second order differentiation with randomly chosen horizontal or vertical orientation (right).*

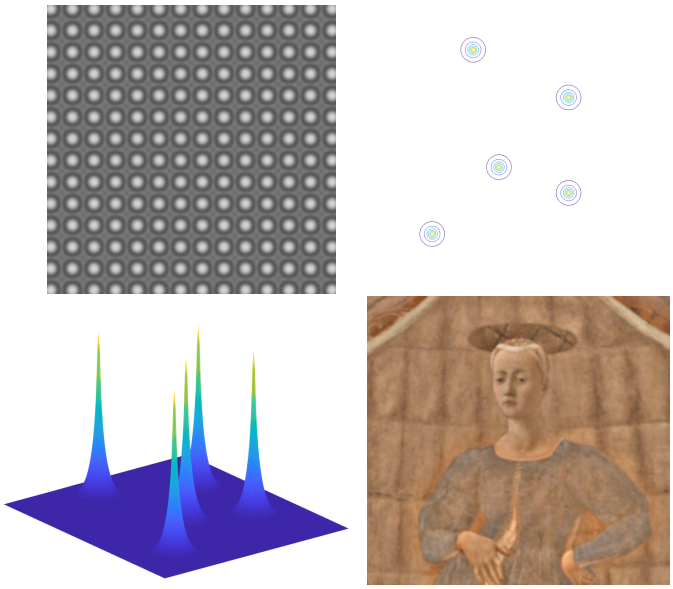

Figure 5. *Classical Laplacians. Upper left: Ps are visualized in a subsampled set of points. Upper right: Level lines of the fundamental solution sampled in some points. Bottom left: Surface of the fundamental solution. Bottom right: Reconstructed image.*

the case of classic Laplacians the Green function in two dimensions is analytically known, $\Gamma(r) = \log(r)$, where $r = \sqrt{x_1^2 + x_2^2}$.

If $a_1 = 0, a_2 = 1, a_3 = 0$, and $\theta = 0$ in every point, then the set of operators is constituted by directional derivatives with all the same orientation (Figure 6) and the corresponding parabolic equation is

$$u_t = \partial^2_{x_1 x_1} u - \partial^2_{x_1 x_1} I.$$

The Green function is very anisotropic, and the reconstruction is corrupted by artifacts. This is due to the fact that many one-dimensional Poisson problems are solved independently in the direction of the derivations, and solutions are uncorrelated.

The case with a mixture of directional derivatives changing from point to point in the horizontal and vertical directions, considered in Figure 7, is very different. As in the previous case, $a_1 = 0, a_2 = 1, a_3 = 0$, but now direction θ is randomly chosen depending on the position $x = (x_1, x_2)$ with values $\theta = 0$ or $\theta = \pi/2$. The result of the differentiation of the stimulus image is shown in Figure 4 (right). Notice that the Green functions of the mixture of operators change from point to point. Although the direction is randomly chosen, the Green function maintains a certain regularity and symmetry. This allows us to obtain a reconstruction of the perceived image without visible artifacts. The formal proof of convergence of this distribution of operators towards classical Laplacians is given in section 5.

A typical distribution of Ps in rodents is a random salt-and-pepper mixture of Mexican hats as well as simple cells with different number of cycles (Figure 8). These correspond to the case where the coefficients a_i are chosen as a partition of the unit such that in any point (x_1, x_2) of the domain Q_ϵ just one parameter has value 1, while the others are null. The choice

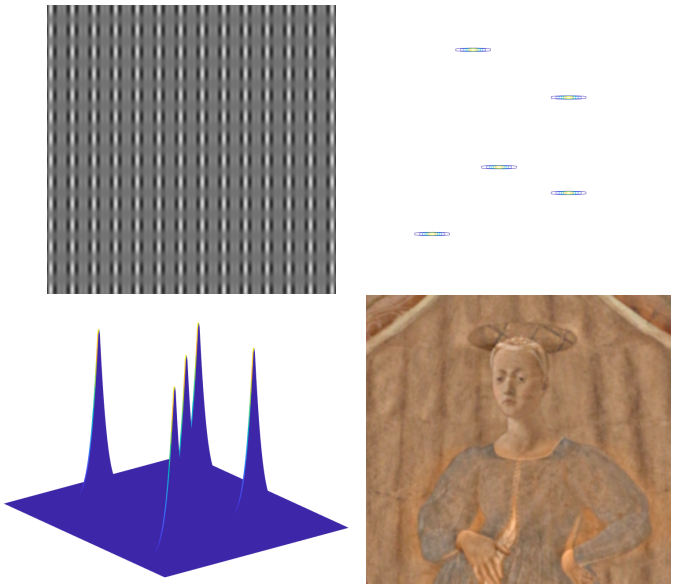

Figure 6. *Homogeneous sub-Riemannian second order operators $L_\Lambda = \partial^2_{x_1 x_1}$. Upper left: Ps are visualized in a subsampled set of points. Upper right: Level lines of the fundamental solution. Bottom left: Surface of the fundamental solution. Notice that fundamental solutions are strongly asymmetric. Bottom right: Reconstructed image: Artifacts appear as uncorrelated horizontal lines.*

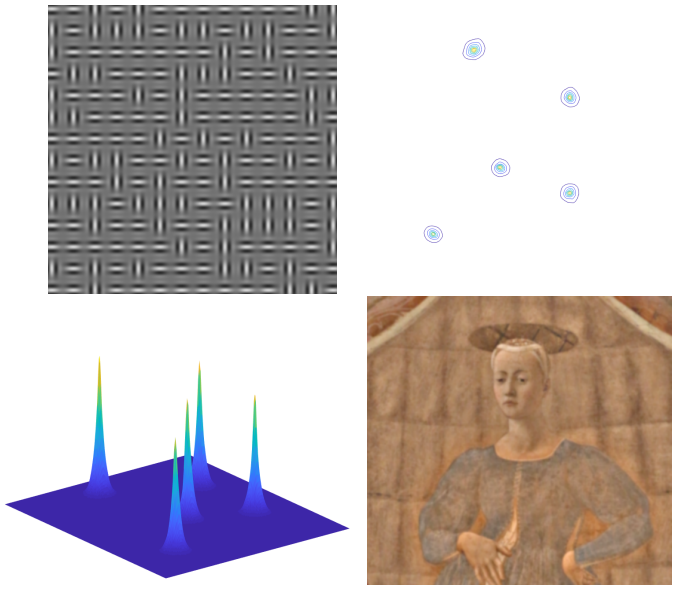

Figure 7. *Sub-Riemannian second order operators in the vertical and horizontal directions. Upper left: Ps are visualized in a subsampled set of points. Upper right: Level lines of the fundamental solution. Bottom left: Surface of the fundamental solution. Notice that fundamental solutions are different point to point and are quite round, although they are composed of anisotropic operators. Bottom right: The reconstructed image appears free from artifacts.*

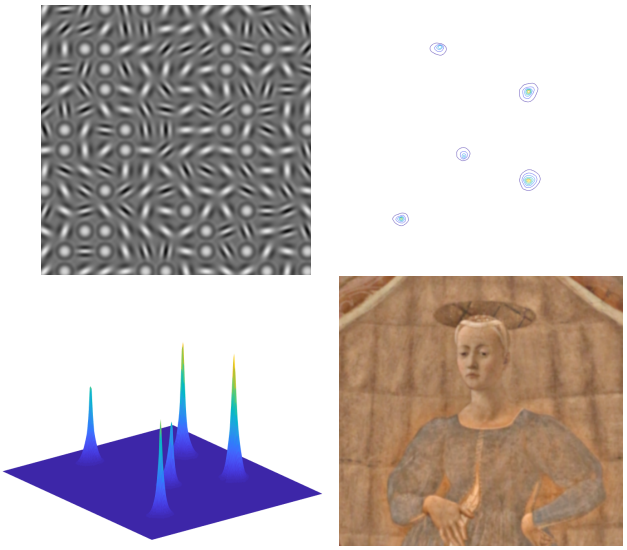

Figure 8. *Heterogeneous operators in the cortex of rodents: Either second or fourth order, Euclidean, or sub-Riemannian operators are randomly distributed with random n-orientations. Upper left: Ps are visualized. Upper right: Level lines of the fundamental solution. Bottom left: Surface of the fundamental solution. Notice that fundamental solutions are different point to point and are quite symmetric, although they are composed of very anisotropic operators of different degree. Bottom right: The reconstructed image appears free from artifacts.*

of the nonnull parameter in every point is random. The distribution of the θ angles is also random over the spatial domain.

Green functions of the mixture are different from point to point and are quite symmetric, although they are composed of very anisotropic operators of different degree. In this case the reconstructed image is the original stimulus $I(x_1, x_2)$ up to a harmonic function, where harmonic means the annulation of the heterogeneous operator $L_\Lambda = 0$. No artifact is visible in the reconstructed-perceived image.

Ps in primates are organized in orientation maps following a pinwheels structure (Figure 9). Also in this case there is a mixture of operators of different orders as on the previous example but with orientations prescribed by the pinwheel structure given by (2.4). Although there is a regularity in the distribution of preferred orientations, the fundamental solutions are very different from those of homogeneous sub-Riemannian second order operators shown in Figure 6. In fact, the presence of a variation of orientation across the domain allows the emergence of weakly anisotropic Green functions. This feature allows for the reconstruction of the perceived image without visible artifacts.

In the following we present a series of simulations on different kind of images with Ps organized as in the cortex of primates. Operators are either second or fourth order, with Euclidean or sub-Riemannian metric. They are randomly distributed with orientations prescribed by the typical pinwheel structure.

In Figure 10 we considered a classical image of simultaneous contrast illusion. In the origin image the background presents a gray level increasing from left to right, and the central

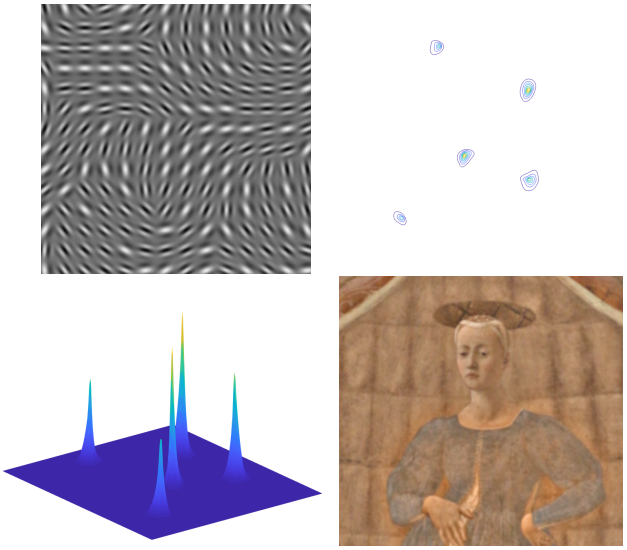

Figure 9. *Heterogeneous operators in the cortex of primates: Operators are either second or fourth order, Euclidean, or sub-Riemannian. They are randomly distributed with orientations prescribed by the typical orientation map of primates (pinwheel structure). Upper left: Ps are visualized. Upper right: Level lines of the fundamental solution. Bottom left: Surface of the fundamental solution. As in the case of rodents, the fundamental solutions are different point to point and quite symmetric. Bottom right: The reconstructed image appears free from artifacts.*

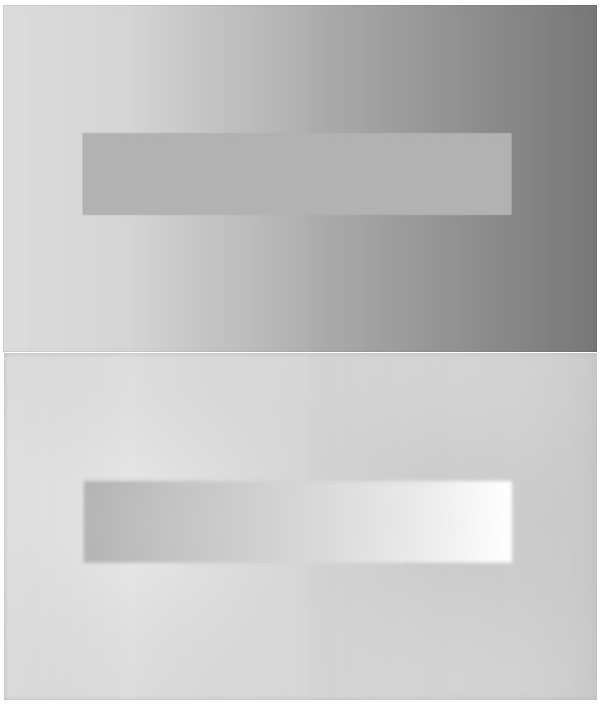

Figure 10. *Simultaneous contrast illusion. Top: Original image. The background presents a linear profile of gray and the central strip has a uniform gray value, but it is perceived as a graded gray level. Bottom: The outcome of simulation shows the graded gray level typical of the perceptual illusion.*

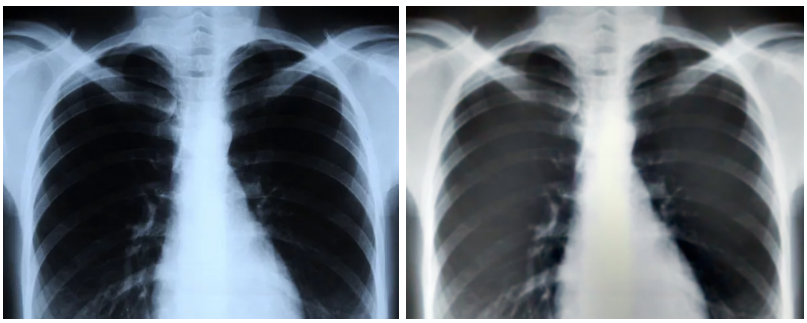

Figure 11. *X-ray test image. Left: Original image. Right: The cortical transform.*

Figure 12. *Upper left: Original image. Upper right: The cortical transform without any parameter. Bottom: The Retinex algorithm proposed in* [31] *with different choice of the* 4 *parameters. Photo by Stephen Wolf.*

Figure 13. *A test image from* [39]. *Top left: Original image. Top right: The best result of the Retinex algorithm proposed in* [39] *after the choice of one parameter. Bottom: The cortical transform without any parameter.* (*Reprinted, with permission, from* [39]).

strip has a uniform gray value, but it is perceived as a graded gray level. The outcome of simulation shows the perceived graded gray level in the occluding strip.

In Figure 11 we considered a medical image. In the reconstructed image the structure of the vertebrae is much clearer.

In Figures 12 and 13 two photographs are considered. The first one was used in [31], where a Retinex algorithm depending by a parameter was proposed. Our image (top right) is comparable with the best result of their algorithm (bottom right), but the algorithm is simpler, since it does not depend on parameters. The fact that it slightly blue is compatible with perceptual laws. In fact, the presence of a yellow part in the stimulus image induces white areas to be perceived with its complementary color, blue. The emergence of antagonistic

pairings of colors correspond to the way our visual system is wired and it is very much supported by the present model.

7. Conclusions. In this paper we have presented a cortical transform model based on the heterogeneous distribution of receptive profiles and the short-range connectivity in the visual cortex. The action of Ps has been expressed via nonnegative operators with random coefficients (random metric and order), the connectivity inverts their action, and the resulting cortical transform corresponds to a heterogeneous Poisson equation. Our main result is that the reconstruction of the perceived image is possible even in the presence of a totally heterogeneous operator whose order varies from one point to another. We provide here a formal proof of the convergence of the operator with random coefficients only in the special case of second order operator; in this case we prove convergence to a deterministic isotropic Laplacian. But other possibilities are at stake. For mixed order operators the experimental results are convincing even if a homogenization theory is still lacking. All these possibilities will be the object of further work in the future.

REFERENCES

[1] S. Abbasi-Sureshjani, M. Favali, G. Citti, A. Sarti, and B. M. ter Haar Romeny, *Curvature integration in a 5D kernel for extracting vessel connections in retinal images*, IEEE Trans. Image Process., 27 (2018), pp. 606–621.

[2] A. Ambrosetti and A. Malchiodi, *Nonlinear Analysis and Semilinear Elliptic Problems*, Cambridge University Press, 2006.

[3] D. Barbieri, G. Citti, G. Cocci, and A. Sarti, *A cortical-inspired geometry for contour perception and motion integration*, J. Math. Imaging Vision, 49 (2013), pp. 511–529.

[4] D. Barbieri, *Reconstructing group wavelet transform from feature maps with a reproducing kernel iteration*, Front. Comput. Neurosci., 16 (2022), https://doi.org/10.3389/fncom.2022.775241.

[5] E. J. Bekkers, R. Duits, A. Mashtakov, and G. Sanguinetti, *A PDE approach to data-driven sub-Riemannian geodesics in SE* (2), SIAM J. Imaging Sci., 8 (2015), pp. 2740–2770, https://doi.org/10.1137/15M1018460.

[6] Bart M. ter Haar Romeny, *Front-end Vision and Multi-scale Image Analysis*, Springer, 2004.

[7] A. Barton and S. Mayboroda, *Higher-order elliptic equations in non-smooth domains: A partial survey, in Harmonic Analysis, Partial Differential Equations, Complex Analysis, Banach Spaces, and Operator Theory, Vol.* 1, Assoc. Women Math. Ser. 4, Springer, 2016, pp. 55–121.

[8] E. Baspinar, A. Sarti, and G. Citti, *A sub-Riemannian model of the visual cortex with frequency and phase*, J. Math. Neurosci., 10 (2020), 11.

[9] F. Bertoni, G. Citti, and A. Sarti, *LGN-CNN: A biologically inspired CNN architecture*, Neural Netw., 145 (2021), pp. 42–55.

[10] F. Bertoni, N. Montobbio, A. Sarti, and G. Citti, *Emergence of Lie symmetries in functional architectures learned by CNNs*, Front. Comput. Neurosci., 15 (2022), https://doi.org/10.3389/fncom.2021.694505.

[11] T. Bonhoeffer and A. Grinvald, *Iso-orientation domains in cat visual cortex are arranged in pinwheel-like patterns*, Nature, 353 (1991), pp. 429–431.

[12] W. H. Bosking, Y. Zhang, B. Schofield, and D. Fitzpatrick, *Orientation selectivity and the arrangement of horizontal connections in tree shrew striate cortex*, J. Neurosci., 17 (1997), pp. 2112–2212.

[13] J. D. Cowan and P. C. Bressloff, *Visual cortex and the Retinex algorithm*, in Human Vision and Electronic Imaging VII, Proc. SPIE 4662, SPIE, 2002, https://doi.org/10.1117/12.469524.

[14] G. Citti, M. Manfredini, and A. Sarti, *Neuronal oscillations in the visual cortex: Γ-convergence to the Riemannian Mumford–Shah functional*, SIAM J. Math. Anal., 35 (2004), pp. 1394–1419, https://doi.org/10.1137/S0036141002398673.

[15] G. Citti and A. Sarti, *A cortical based model of perceptual completion in the roto-translation space*, J. Math. Imaging Vision, 24 (2006), pp. 307–326.
[16] G. Citti and A. Sarti, *A gauge field model of modal completion*, J. Math. Imaging Vision, 52 (2015), pp. 267–284.
[17] G. Citti and A. Sarti, *Neuromathematics of Vision*, Springer, Berlin, 2014.
[18] G. Citti and N. Garofalo E. Lanconelli, *Harnack's inequality for sum of squares of vector fields plus a potential*, Amer. J. Math., 115 (1993), pp. 699–734.
[19] A. Das and C. D. Gilbert, *Topography of contextual modulations mediated by short-range interactions in primary visual cortex*, Nature, 399 (1999), pp. 655–661.
[20] E. De Giorgi, *Sulla convergenza di alcune successioni d'integrali del tipo dell'area*, Rend. Mat. (6), 8 (1975), pp. 277–294.
[21] E. De Giorgi, *G-operators and Γ-convergence*, Proc. Int. Congress Math. Warszawa, 414 (1983), pp. 1175–1191.
[22] G. C. DeAngelis, A. Anzai, and R. D. Freeman, *Receptive field dynamics in the central visual pathways*, Trends Neurosci., 18 (1995), pp. 451–457.
[23] G. C. DeAngelis and A. Anzai, *A modern view of the classical receptive field: Linear and non-linear spatio-temporal processing by V1 neurons*, in The Visual Neurosciences, Vol. 1, L. M. Chalupa and J. S. Werner, eds., MIT Press, 2004, pp. 704–719.
[24] D. Gilbarg and N. S. Trudinger, *Elliptic Partial Differential Equations of Second Order*, Classics in Math. 224, Springer, 2001.
[25] D. H. Hubel and T. N. Wiesel, *Receptive fields of single neurones in the cat's striate cortex*, J. Physiol., 147 (1959), pp. 226–238.
[26] D. H. Hubel and T. N. Wiesel, *Receptive fields, binocular interaction and functional architecture in the cat's visual cortex*, J. Physiol., 160 (1962), pp. 106–154.
[27] D. H. Hubel and T. N. Wiesel, *Brain and Visual Perception: The Story of a 25-Year Collaboration*, Oxford University Press, 2005.
[28] J. Jones and L. Palmer, *The two-dimensional spatial structure of simple receptive fields in cat striate cortex*, J. Neurophysiol., 58 (1987), pp. 1187–1211.
[29] J. Jones and L. Palmer, *An evaluation of the two-dimensional Gabor filter model of simple receptive fields in cat striate cortex*, J. Neurophysiol., 58 (1987), pp. 1233–1258.
[30] M. Kaschube, *Neural maps versus salt-and-pepper organization in visual cortex*, Curr. Opin. Neurobiol., 241 (2014), pp. 95–102.
[31] R. Kimmel, M. Elad, D. Shaked, R. Keshet, and I. Sobel, *A variational framework for Retinex*, Internat. J. Comput. Vision, 52 (2003), pp. 7–23.
[32] J. J. Koenderink, *The structure of images*, Biol. Cybernet., 50 (1984), pp. 363–370.
[33] J. J. Koenderink and A. J. van Doorn, *Representation of local geometry in the visual system*, Biol. Cybernet., 55 (1987), pp. 367–375.
[34] S. M. Kozlov, *Averaging of difference schemes*, Math. USSR Sb., 57 (1987), pp. 351–369.
[35] T. Lindeberg, *A computational theory of visual receptive fields*, Biol. Cybernet., 107 (2013), pp. 589–635.
[36] W. Littman, G. Stampachia, and H. Weinberger, *Regular points for elliptic equations with discontinuous coefficients*, Ann. Sc. Norm. Sup. Pisa, 17 (1963), pp. 45–79.
[37] S. Marcelja, *Mathematical description of the responses of simple cortical cells*, J. Opt. Soc. Amer., 70 (1980), pp. 1297–1300.
[38] M. Martinez-Garcia, P. Cyriac, T. Batard, M. Bertalmío, and J. Malo, *Derivatives and inverse of cascaded linear+nonlinear neural models*, Plos ONE, 13 (2018), e0201326.
[39] J. M. Morel, A. B. Petro, and C. Sbert, *A PDE formalization of Retinex theory*, Trans. Image Process., 19 (2010), pp. 2825–2837.
[40] G. C. Papanicolaou and S. R. S. Varadhan, *Diffusions with random coefficients*, in Statistics and Probability, G. Kallianpur, P. Krishnaiah, and J. K. Ghosh, eds., North-Holland, 1982, pp. 547–552.
[41] S. Peron, R. Pancholi, B. Voelcker, J. D. Wittenbach, H. F. Ólafsdóttir, J. Freeman, and K. Svoboda, *Recurrent interactions in local cortical circuits*, Nature, 579 (2020), pp. 256–259.
[42] J. Petitot, *The neurogeometry of pinwheels as a sub-Riemannian contact structure*, J. Physiol.-Paris, 97 (2003), pp. 265–309.

[43] A. Piatnitski and E. Remy, *Homogenization of elliptic difference operators*, SIAM J. Math. Anal., 33 (2001), pp. 53–83, https://doi.org/10.1137/S003614100033808X.
[44] D. L. Ringach, *Spatial structure and symmetry of simple-cell receptive fields in macaque primary visual cortex*, J. Neurophysiol., 88 (2002), pp. 455–463.
[45] R. W. Rodieck, *Quantitative analysis of cat retinal ganglion cell response to visual stimuli*, Vis. Res., 5 (1965), pp. 583–601.
[46] L. P. Rothschild and E. M. Stein, *Hypoelliptic differential operators and nilpotent groups*, Acta Math., 137 (1976), pp. 247–320.
[47] A. Sarti, G. Citti, and M. Manfredini, *From neural oscillations to variational problems in the visual cortex*, J. Physiol.-Paris, 97 (2003), pp. 379–385.
[48] A. Sarti, G. Citti, and J. Petitot, *The symplectic structure of the primary visual cortex*, Biol. Cybernet., 98 (2008), pp. 33–48.
[49] A. Sarti, G. Citti, and D. Piotrowski, *Differential heterogenesis and the emergence of semiotic function*, Semiotica, 230 (2019), pp. 1–34.
[50] A. Sarti, G. Citti, and D. Piotrowski, *Differential Heterogenesis: Mutant Forms, Sensitive Bodies*, Springer-Nature, 2022.
[51] S. Spagnolo, *Sulla convergenza di soluzioni di equazioni paraboliche ed ellittiche*, Ann. Scuola Norm-SCI., 22 (1968), pp. 571–597.
[52] J. C. Strikwerda, *Finite Difference Schemes and Partial Differential Equations*, 1st ed., Chapman & Hall, 1989.
[53] R. A. Young, *The Gaussian derivative model for spatial vision:* I. *Retinal mechanisms*, Spat. Vision, 2 (1987), pp. 273–293.
[54] R. A. Young, R. M. Lesperance, and W. W. Meyer, *The Gaussian derivative model for spatio-temporal vision:* I. *Cortical model*, Spat. Vision, 14 (2001), pp. 261–319.
[55] R. A. Young and R. M. Lesperance, *The Gaussian derivative model for spatio-temporal vision:* II. *Cortical data*, Spat. Vision, 14 (2001), pp. 321–389.